HHS Public Access

Author manuscript

Biomaterials. Author manuscript; available in PMC 2016 May 01.

Published in final edited form as:

Biomaterials. 2015 May ; 50: 115–126. doi:10.1016/j.biomaterials.2015.01.045.

Arterial grafts exhibiting unprecedented cellular infiltration and remodeling in vivo: the role of cells in the vascular wall

Sindhu Row[1], **Haofan Peng**[1], **Evan M. Schlaich**[1], **Carmon Koenigsknecht**[3], **Stelios T. Andreadis**[1,2,4,*], and **Daniel D. Swartz**[3,4,*]

[1]Department of Chemical and Biological Engineering, University at Buffalo, State University of New York, Amherst, NY 14260-4200

[2]Department of Biomedical Engineering, University at Buffalo, State University of New York, Amherst, NY 14260-4200

[3]Department of Pediatrics, Women and Children's Hospital of Buffalo, University at Buffalo, State University of New York, Amherst, NY 14260-4200

[4]Center of Excellence in Bioinformatics and Life Sciences, University at Buffalo, State University of New York, Amherst, NY 14260-4200

Abstract

Objective—To engineer and implant vascular grafts in the arterial circulation of a pre-clinical animal model and assess the role of donor medial cells in graft remodeling and function.

Approach and results—Vascular grafts were engineered using Small Intestinal Submucosa (SIS)-fibrin hybrid scaffold and implanted interpositionally into the arterial circulation of an ovine model. We sought to demonstrate implantability of SIS-Fibrin based grafts; examine the remodeling; and determine whether the presence of vascular cells in the medial wall was necessary for cellular infiltration from the host and successful remodeling of the implants. We observed no occlusions or anastomotic complications in 18 animals that received these grafts. Notably, the grafts exhibited unprecedented levels of host cell infiltration that was not limited to the anastomotic sites but occurred through the lumen as well as the extramural side, leading to uniform cell distribution. Incoming cells remodeled the extracellular matrix and matured into functional smooth muscle cells as evidenced by expression of myogenic markers and development of vascular reactivity. Interestingly, tracking the donor cells revealed that their presence was beneficial but not necessary for successful grafting. Indeed, the proliferation rate and number of donor cells decreased over time as the vascular wall was dominated by host cells leading to significant remodeling and development of contractile function.

[*]Address for all Correspondence: Daniel D. Swartz, Department of Pediatrics, Women and Children's Hospital of Buffalo; swartzda@buffalo.edu Or Stelios T. Andreadis, Bioengineering Laboratory, 908 Furnas Hall, Department of Chemical and Biological Engineering University at Buffalo, State University of New York; sandread@buffalo.edu.

No disclosable conflicts of interest.

Conclusions—These results demonstrate that SIS-Fibrin grafts can be successfully implanted into the arterial circulation of a clinically relevant animal model, improve our understanding of vascular graft remodeling and raise the possibility of engineering mural cell-free arterial grafts.

Keywords

Vascular graft; tissue engineered artery; ovine animal model; small intestinal submucosa; hair follicle stem cells; cell-free medial layer

INTRODUCTION

Treatment of arterial obstructions by autologous vascular grafting has several technical and patient-related risks [1]. In contrast to synthetic substitutes that faced complications with compatibility and biological function, cell-seeded tissue engineered vessels (TEVs) have been shown to perform better at the blood-material interface [2]. Biopolymers like fibrin and collagen have been employed successfully as venous conduits but their mechanical properties need to be improved for use as arterial substitutes [3, 4]. Decellularized vessels originating either from native arteries or cell-seeded engineered tissues have gained attention recently as they may be more readily available; they possess native-like ECM composition and mechanical properties enabling implantation and remodeling *in-vivo* [5–7]. However, several challenges remain. Decellularized TEVs exhibit limited host cell infiltration, mostly from the anastomotic sites, resulting in slow matrix remodeling and inadequate vascular function even several months post-implantation. In addition, the role of donor cells in promoting host cell infiltration and long-term fate after implantation is not well understood.

Endothelial cells (ECs) have been shown to be necessary to maintain an anti-thrombogenic lumen and graft patency *in-vivo* [6]. Using an arterio-venous shunt bypass model, our group demonstrated that in the absence of an endothelial monolayer, platelet deposition occurred within 30 minutes of exposure of SIS-Fibrin vascular grafts to the circulation of an ovine animal model [8]. While we established the necessity for EC coverage in the lumen, it was not clear whether the presence of medial cells in the vascular wall was required for successful remodeling of TEVs. One study suggested that the presence of SMCs was necessary to provide a physiological architecture and boost remodeling and contractile function of vascular grafts based on decellularized arteries [7]. In another elegant study, TEVs were generated by seeding human allogeneic SMCs onto poly-glycolic acid scaffolds and allowed to grow for 10 weeks under mechanical stimulation to boost ECM secretion and remodeling. The TEVs were then decellularized, seeded with autologous ECs and implanted successfully in the arterial circulation of baboons and dogs, where they remained patent for several months [5]. However, host cell infiltration and ECM remodeling were limited and occurred predominantly near the anastomotic sites. In recent studies, synthetic grafts completely devoid of cells have been attempted. However, the problem of neointimal hyperplasia could not be overcome [9]. Two recent studies showed that TEVs lacking cells in the vascular wall could be implanted into the venous system of mice [10] or the abdominal aorta of rats [11]. However, it is not clear that these results can be extrapolated to a more physiologically relevant animal model. Hence, we designed this study to evaluate the performance of TEVs made with only ECs in the lumen (denoted as EC TEVs) vs. those that

also contained SMC within the vascular wall (denoted as EC/SMC TEVs). A total of n=18 grafts were implanted and evaluated at 1 week, 1 month and 3 months post-implantation.

SIS has been shown to retain a porous scaffold suitable for tissue reconstruction, enabling cell migration and proliferation in a wide range of applications including vascular grafts and patches [12–14], ileum repair [15], diaphragm regeneration [16], rotator cuff replacements [17]. Here, we employed SIS that was turned into cylindrical grafts using fibrin glue, which also served as donor mural cell scaffold. When implanted into the carotid arteries of sheep, SIS-Fibrin vascular grafts exhibited long-term patency and high levels of host cell infiltration, leading to cell density in the vascular wall that was similar to that of native arteries as soon as 1 mo post-implantation. Initially, the grafts were invaded by monocytes from the blood and extramural wall. Within one month post-implantation, α-smooth muscle actin and calponin-expressing cells dominated the tissues leading to development of considerable vascular contractility, which in some cases reached the levels of native arteries. Interestingly, the presence of donor cells was helpful but not necessary for successful host cell infiltration, remodeling or development of vascular function. Our results improve our understanding of vascular graft remodeling into the arterial circulation of a large animal model. They also demonstrate that even in the absence of mural cells in the vascular wall, SIS-Fibrin grafts can be used successfully as arterial substitutes, paving the way for engineering highly functional arteries with reduced complexity and shorter preparation times.

MATERIALS AND METHODS

Graft manufacture

Hydrated SIS (Cook Biotech, West Lafayette IN), cut into sheets (6 mm × 8 mm) was rolled manually to obtain cylindrical grafts (Fig. S1A) as described before [8]. A previously optimized concentration of 22 mg/mL fibrinogen (Enzyme Research Laboratories, South Bend, IN) and 125 U/mL thrombin (Sigma, St Louis, MO) was used to as cell scaffold as well as to glue the SIS layers together yielding grafts that could hold burst pressures of up to 1200 ± 250 mmHg. Grafts in the EC/SMC group were modified by addition of Hair Follicle Mesenchymal Stem Cell derived Smooth Muscle Cells (HF-SMCs) in 1 ml of fibrin glue (10 million cells per graft). HF-SMCs were obtained as previously described from single hair follicles of full thickness skin from male sheep [18]. Passage 4 cells were transduced with αSMA-EGFP (α-Smooth Muscle Actin-Enhanced Green Florescence Protein) recombinant lentivirus in the presence of 8 mg/mL polybrene and EGFP+ cells were subsequently sorted using fluorescence-activated cell sorting and were used between passages 11 to 21. The resulting SIS-Fibrin grafts were incubated at 37°C for 30 min to allow for fibrin polymerization. After polymerization, SIS-Fibrin grafts were gently detached from the PDMS (PolyDiMethyl-Siloxane) coated mandrel and the two ends of the grafts were cut to exclude any incomplete layers.

After transferring and fastening the grafts in bioreactor chambers (Fig. S1B, Tissue Growth Technologies, TGT (Instron, Norwood MA)), OPAECs (Ovine Pulmonary Artery Endothelial Cells, obtained from neonatal sheep) were trypsinized and injected into the lumen of each graft (2×10^6 cells/mL, 5 mL/graft). Bioreactor chambers were placed in a

rotary device at 5 RPM (Roto-shake-genie, Bohemia, NY) overnight. Following seeding, the grafts were incubated at 37°C for 3 days to enhance OPAEC adherence and confluence at static pressure providing continuous distention. For preconditioning the samples, chambers were connected to the flow system (Fig. S1C). The wall shear stress was calculated by Hagen-Poiseuille equation, and corresponding volumetric flow rates were used to program the pump of the bioreactor:

$$t_w = 4\frac{\mu Q}{\pi R3}$$

A shear stress ramping protocol was used over 4 days to a final shear stress of 6 dynes/cm^2 (Fig. S1D).

Animal care and graft implantation

Procedures and protocols in this study were approved by the IACUC (Institutional Animal Care and Use Committee) of the State University of New York at Buffalo. A total of 20 adult female Dorset Cross sheep between the ages of 2–4 years and weighing 35–50 kg were used. Anesthesia was induced via diazepam and ketamine mixture, or teletamine and zolazepam mixture IV. Anesthesia was maintained with isoflurane through an endotracheal tube using a positive pressure ventilator and 100% oxygen. Cyclosporine A (200 mg/day), aspirin (975 mg/day), and coumadin (20–30 mg/day) were administered to the animals, starting 3 days prior to the procedure and continued for the duration of the study. Heparin (100 unit/kg) was administered intravenously to the animals 30 minutes prior to clamping of the artery and then infused at a rate of 100 U/kg/hr. throughout the surgery. Before implantation, we monitored the heart rate of each animal and the flow rate in the native vessel, which ranged between 170–280 ml/min.

The TEVs (4–5 cm in length) were implanted as interpositional grafts into the left common carotid artery of 2 to 4 year old female sheep. An ultrasonic flow probe was placed temporarily at a distal site, to measure the blood flow rate before and after grafting procedure. Recoil along longitudinal direction was assessed and additional 1.5–1.8 mm of native vessel was removed accordingly to maintain similar longitudinal tension to native vessel. Each TEV was pre-soaked in heparinized saline and anastomosed into the native carotid using end-to-end interrupted suture technique with 10–12 stitches on both proximal and distal ends (Fig. S1E–F). After the TEV was in place, the native vessel was unclamped and the flow rate through the graft was monitored for at least 30 minutes until it stabilized, typically at higher values than the flow rate measured in the native vessel (220–470 ml/min, Supplementary Video V1). We implanted a total of 20 animals, two of which died of reasons unrelated to the implants. All the data reported in this study are from n=18 successfully implanted animals, representing n=3 per condition (EC, EC/SMC) and time point (1 week-1 wk, 1 month-1 mo, 3 months-3 mo).

International Normalized Ratio (INR) was monitored and maintained between 1.7–2.5 after 5–8 days of Coumadin medication (Alere Home Monitoring, Inc., Livermore, CA). Animals

were on controlled diet (1.8 kg grain and 0.4 kg hay) during the recovery time and typically gained 8–12 kg.

Doppler ultrasound

Directional color power Doppler ultrasonography (ultrasound-180 plus, Sonosite, WA, USA) was performed bi-weekly to determine graft patency. We obtained measurements of diameters and flow rate of both carotids and the measurement of the right (control) carotid served to normalize the data. Normalized flow rates and diameters of each animal were then averaged over time and reported as average ± SD (Standard Deviation).

Angiography

In order to image dynamic flow characteristics in the graft and quantify diameters, three-dimensional rotational angiography was performed post-implantation on weeks 4 and 12 in a Toshiba angiography suite (Dicom Viewer, Infinix, and Vx-i). A 4-Fr angiocath sheath was inserted into the femoral artery and placed in the aortic arch for contrast injection. Size calibration was achieved by placing beads of 4.65 mm diameter in the anaesthetized animal and imaging them simultaneously with the carotid vessels. A scaling factor, thus obtained was used to measure the diameter of control and graft vessels.

Euthanasia and explantation of tissues

At times indicated, animals were euthanized using 5.85 g of pentobarbital sodium (Fatal Plus, Vortech Pharmaceuticals, Dearborn MI). Both carotids were excised and cleaned extensively by rinsing with heparinized saline through the lumen. Connective tissue and fibrosis were trimmed off and ring sections were cut from the center of the TEV or native vessels to test for vaso-reactive function and mechanical properties. The remaining tissues were pressure fixed using 10% neutral buffered formalin for histological analysis, IHC (ImmunoHistoChemistry) and Scanning Electron Microscopy (SEM).

Vascular reactivity

Ring sections of explanted TEVs and native arteries (n=3 for each) were connected to a force transducer and suspended in a tissue bath containing Krebs-Ringer solution with constant oxygen supply (94% O_2, 6% CO_2). After equilibrating sections at a basal force of 2.0 g, vaso-active agonists, namely (i) Endothelin-1 (ET-1, 10^{-8}M); (ii) U46619 (2×10^{-7}M); and (iii) KCl (118 mM) were added to the baths and the resultant isometric constriction forces were recorded using a PowerLab data acquisition unit and analyzed by Chart5 software (ADInstruments, Colorado Springs, CO). Relaxing agents, namely, SNAP(Sodium Nitro Prusside and ROCK inhibitor Y27632 were then added to bring vessels back to their basal tone. Washes were performed with Krebs-Ringer solution to ensure removal of vaso-active agonist or relaxant before proceeding to the next step. Data was reported as force exerted by tissue per unit area of tissue (N/m^2 or Pa).

Mechanical properties

Pre-implanted and explanted SIS-Fibrin grafts and native common carotid arteries were assessed for mechanical properties using a uniaxial Intron tensile tester (Model 3343, 50 N

load cell, Instron Corporation, Norwood, MA). Ring samples were mounted onto stainless steel hooks and inserted into tester grips. Samples were displaced uniaxially at constant speed (18 mm/min crosshead speed) until failure. Length-tension curves were obtained during displacement and normalized into stress-strain relationships. The Young's Modulus was calculated as the linear slope of the stress-strain curve devoid of slack related off-sets due to errors in sample engagement and initial length values. UTS (Ultimate Tensile Strength) was calculated as the breaking force per unit area of tissue and expressed in MPa.

Histology and IHC

Pressure fixed samples were dehydrated in a series of graded ethanol solutions, xylene substitutes and then embedded in paraffin as reported elsewhere [4, 19]. For histological evaluation, 5μm paraffin embedded tissue sections were stained with Harris H&E (Haematoxylin and Eosin). The numbers of infiltrated cells in explanted tissues were assessed using ImageJ software (NIH, USA, *rsbweb.nih.gov/ij/)*. Histological cross-section images were converted to gray scale and thresholded to discriminate the background from cell nuclei. To assess the number of cells within each explant, particle analysis was employed. Particles with projected area ranging from 5–200μm^2 were counted regardless of circularity. Cell counts were normalized based on the area of the tissue in each field of view. A total of 5 fields (containing to 500–1000 cells) were counted for each animal and cell densities were represented in cell#/mm^2. For quantification of collagen in Masson's trichrome images, Image J was used to separate the RGB channels in each image. Then the intensity of the blue channel was quantified, normalized to the area and reported as percent of the corresponding average value of native artery (n=8).

Following de-paraffinization and antigen retrieval, IHC was performed using the following antibodies (1:100) in PBS containing 5% normal goat serum (Sigma-Aldrich Co., St. Louis, MO): (i) Calponin (Santa Cruz Biotechnology, Inc. Dallas, TX), (ii) CD144 or VE-Cadherin (Cell Signaling Technology, Boston, MA), (iii) Anti-SRY (Sigma-Aldrich, St. Louis, MO), (iv) AIF(Allograft Inflammatory Factor or anti-Iba-I (Wako Chemicals USA, Richmond, VA), (v) PCNA (BioLegend, London, UK) (vi) MYH11 (Biomedical Technologies Inc., Alfa Aesar, Ward Hill, MA) and (vii) eNOS/NOS type III (BD biosciences, San Jose, CA). After overnight incubation at 4°C, corresponding secondary antibodies were used in 1:200 dilution for 1 hour at room temperature. Cell nuclei were counterstained with DAPI (Hoechst 33342; 10 mg/ml; 1:200 dilution; 5 min at room temperature; EMD Millipore Laboratory Chemicals, Billerica, MA).

SEM

SEM (S4000; Hitachi, Tokyo, Japan) was employed to evaluate EC morphology and assess the luminal surface of the SIS-Fibrin grafts post-implantation. Briefly, fixed samples were dehydrated in a sequence of ethanol solutions for 5 minutes each and incubated in hexamethyl-disilazane (MP Biomedicals, Solon, OH) for 15 minutes. After air-drying at room temperature, the samples were coated with a 20 nm layer of evaporated gold and processed for imaging.

TUNEL assay

TUNEL assay was performed on paraffin sections of explanted tissues using the Apo-Alert DNA Fragmentation Assay Kit (Clontech) following manufacturer's instructions. TUNEL positive nuclei were then counted using Image J software, and expressed as a percentage of total nuclei counted from DAPI staining.

Quantification of IHC and TUNEL assay

Images with positive cells in a particular channel were converted to grayscale and cells were counted using Image J software. For each graft (animal), we counted cells in n=4–5 fields of view. With n=3 animals (grafts) per group (EC or EC/SMC at each time point), at least 500 cells were analyzed for each group. Statistical analysis was performed as described before. The channel for DAPI was used to obtain the total cell number per sample.

Statistical Analyses

Values are means ± SD. Significant differences between animal groups were determined by Student's *t*-test (paired, two-tailed) or ANOVA (Analysis of Variance) with post-hoc analysis using Student–Newman–Keuls multiple comparison test or Spearman correlations analysis. Values of $P \leq 0.05$ were accepted as significant. Five (n=5) fields of view (for IHC) or n=3 ring samples (for vaso-reactivity or mechanical properties) were independently evaluated for each animal.

RESULTS

Assessment of Graft Patency by Ultrasonography Indicates Bilateral Carotid Flow

Vascular grafts containing both cell types were termed EC/SMC TEVs, while those without SMC in the vascular wall were termed EC TEVs. Evaluation of patency of implanted TEVs by directional color Doppler ultrasound was performed bi-weekly by monitoring carotid diameters, pulsatility and flow velocities. In order to remove undesirable dependencies on the physical state of the non-sedated animal, all flow volume and diameter measurements on the left carotid (grafted side) were reported as normalized to the values measured on the right carotid (control side). As shown in Fig. 1A–B, implanted TEVs and native carotids displayed similar characteristic Doppler spectral traces indicating uniform pulsatile flow profiles. The graft diameters and flow volumes per cardiac cycle were normalized to the corresponding values of the right carotid artery in each animal and the normalized values were plotted as a function of time for each group (Fig. S2A–B). The grafts typically showed higher diameters, which was not unexpected as TEVs at implantation normally measured 5.0 ± 0.5 mm on their inner diameter, which was marginally larger compared to native arteries (3.8 ± 0.7 mm). No significant differences in diameters or flow volumes were detected between the EC/SMC and EC groups at 1 mo or 3 mo post-implantation.

Angiographic and Macroscopic Images of TEVs Exhibit no Anastomotic Complications

Angiographic images were taken at the end of 1 mo or 3 mo in both experimental groups to validate patency and confirm consistent blood flow through the implanted TEVs (Supplementary video V2 and V3). Fig. 1C indicates measurements made across the native

carotid, TEV and anastomotic sections. All SIS-Fibrin grafts were patent with no significant stenosis and both groups of TEVs (EC/SMC and EC) demonstrated identical bilateral carotid blood flow as well as absence of turbulence at the anastomotic sites.

Once the animals were euthanized, explanted grafts were cut open to evaluate the lumen for blood deposits. Gross images showed clean lumen at 3 mo in both EC/SMC and EC groups (Fig. 1D). Naturally, fibrosis was observed on the outer surface of the graft, which likely provided mechanical support and served as a source of host cells infiltrating into the graft.

Vascular grafts exhibited high rates of host cell infiltration and uniform cell distribution throughout the vascular wall

H&E staining of complete ring cross-sections showed that the medial layer thickness of EC/SMC and EC grafts at 3 mo was similar to that of native arteries with no indication of hyperplasia in any of the grafts (Fig. 2A). Histological analysis showed robust infiltration of host cells, which increased steadily over time (Fig. 2B). Interestingly, EC/SMC grafts exhibited higher rate of cell infiltration reaching homeostatic cell density (similar to the native vessels) at 1 mo and remained unchanged thereafter (Fig. 2C). However, by 3 mo both groups showed similar cell density with native arteries, suggesting that the SIS-Fibrin scaffold supported very efficient host cell infiltration, which was further facilitated by the presence of donor cells in the engineered vascular wall.

Next we evaluated the distribution of cells throughout the vessel wall over time from the lumen to the extramural wall side. To this end, cross-section images of explanted grafts were divided into 3 equal zones from the lumen to the adventitia as shown in Fig. 2D and the cell density was quantified in each zone (Fig. 2E). At 1 and 3 mo, all zones had nearly equal cell densities in both groups. At 1 wk both groups showed similar cell density in zone 1, suggesting similar rates of cellular infiltration possibly from the graft lumen. However, EC/SMC grafts showed significantly higher cell density in zones 2 and 3, suggesting higher rates of cell infiltration from the surrounding tissue than the EC grafts.

We also determined the cell density as a function of position along the length of the grafts, from one anastomotic site to the other. To this end, the cell density in each graft was determined near each of the suture site zones (proximal and distal) as well as the longitudinal mid-section of the graft as shown in the schematic (Fig. 2F). Notably, the cell density was similar in each zone, indicating uniform cell distribution throughout the length of each graft (Fig. 2F). Collectively, these data suggested that host cell infiltration did not occur only from the anastomotic ends but also through the luminal and adventitial sides of the implants. Interestingly, we also observed development of vaso-vasorum in the adventitial tissue as shown by the appearance of microvessels filled with red blood cells (arrows in Fig. S3).

The collagen content of the grafts was evaluated by Masson’s Trichrome staining (Fig. 2G) and the staining intensity was quantified using Image J (Fig. 2H). EC/SMC TEVs exhibited significantly higher collagen content at all time points, possibly as a result of higher cell infiltration rates or faster maturation of the infiltrated host cells. Collagen synthesis increased over time in both groups, indicating continued remodeling by the host cells.

However, even at 3 mo, neither group had reached the fibrillar organization observed in the native arteries, suggesting that the tissues were not completely remodeled by the 3 mo time point.

Explanted TEVs Show Similar Structure as Native Arteries

To further characterize the infiltrated cells, IHC was performed on paraffin cross-sections of explanted grafts from both groups at 3 mo. Medial layer cells in the graft stained positive for Calponin (CNN1, red) and cells on the luminal surface stained positive for VE-Cadherin (CD144, green) (Fig. 3A). SEM was performed to image the microscopic properties of the lumen. At 1 mo and 3 mo, all grafts displayed a homogenous endothelialized lumen, with no platelet aggregates or blood cell deposits anywhere on the luminal surface (Fig. 3B). The cell bodies also appeared to be oriented in the direction of flow. These results further confirmed graft patency and the anti-thrombogenic properties of the mature luminal surface. In addition, immunostaining for eNOS (endothelial Nitric Oxide Synthase) using an antibody specific to the C-terminus domain, which is required for phosphorylation and activity of the mature protein [20], suggested that the endothelial monolayer was functional (Fig. S4).

Immuno-staining for α-SMA and MYH11 showed the presence of fibers by 1 mo in vivo, which developed into mature organized filamentous fibers comparable to those of native arteries by 3 mo (Fig. 3C–D). These results indicated significant graft maturation over time within the host.

TEVs developed contractile function over time *in-vivo*

Next we examined the vascular contractility of the implants in response to vaso-active agonists, U46619, Endothelin-1 and KCl by measuring the isometric tension exerted by ring sections of explanted grafts at 1 and 3 mo post-implantation. At 1 mo *in-vivo*, no contractile force was measured in either group. Notably, at 3 mo, the response of both EC and EC/SMC grafts to U46619 was similar to that of native arteries (native artery response to U46619: 335.69±87.8 KPa, $p>0.5$, compared to EC or EC/SMC grafts, n=3) (Fig. 4A). Both groups also showed similar response to ET-1 and KCl, albeit significantly lower than those of native arteries (native artery response to ET1: 3,260.3 ± 314.3 KPa; or KCl: 10,416.9 ± 286.2 KPa, n=12, $p<0.05$). Signature responses upon addition of vaso-active reagents are shown in Fig. 4B. Interestingly, not only did the vessels respond to constrictive agents, but also relaxed in response to the ROCK inhibitor, Y27632 and the nitric oxide donor, SNAP. Signature response to SNAP is shown in Fig. 4B. A ~30% relaxation was seen in response to SNAP as compared to ~58% relaxation exhibited by the native arteries (Fig 4C). Since the EC grafts displayed similar levels of vascular contractility as EC/SMC grafts at 3 mo post-implantation, the contractile function might be the result of host-cell infiltration and maturation to smooth muscle *in-vivo* within the SIS-Fibrin scaffolds.

Mechanical Properties of implanted TEVs

Tissue rings were excised from graft explants, mounted on a force transducer and stretched incrementally until they broke, yielding the UTS and Young's Modulus (Fig. 4D–E). Although pre-implanted TEVs exhibited lower mechanical properties as compared to native

arteries, they showed significant gains over time in-vivo. Specifically, at 3 mo post-implantation, SIS-Fibrin explants displayed UTS and Young's modulus that were comparable to those of native arteries. EC/SMC grafts showed a statistical advantage in their Young's modulus, which correlated with higher collagen content.

Evaluation of Donor Cell Retention and Host Cell Infiltration and Proliferation

In order to track the fate of donor cells, TEVs were prepared with male HF-SMCs and implanted into female recipients. Donor cells (male) were identified by an antibody to SRY and cell proliferation was evaluated by PCNA co-staining (Fig. 5A).

Interestingly, over time the percentage of proliferating (PCNA+) cells in the total cell population in EC/SMC grafts decreased modestly from 43.5±8.9% at 1 wk, to 39.5±6.9% at 1 mo to 30.9±2.0% after 3 mo (n=3 for each group) (Fig. 5B), possibly indicating maturation of the cells populating the grafts. On the other hand, the percentage of proliferative cells (PCNA+) in the donor (SRY+) cell population was about 36.2±3.2% at 1 wk and was maintained at similar level at 1 mo (36.3±4.6%) but decreased significantly to 12.8±1.9% after 3 mo in vivo (Fig. 5C). Conversely, only a small percentage of the proliferating (PCNA+) cells stained positive for the Y-chromosome at 1 wk (22.2±3.9%) and 1 mo (16.2±3.7%) and decreased dramatically after 3 mo (2.6±0.7%) (Fig. 5C). As a result, the percentage of donor cells (SRY+) within the vascular wall decreased significantly from 45.5±6.7% at 1 wk to 17.5±6.5% at 1 mo to 8.2±2.6% after 3 mo (Fig. 5B), suggesting that by 3 mo post-implantation the grafts were dominated by highly proliferative host cells.

The decreased number of donor (SRY+) cells prompted us to examine whether in addition to reduced proliferation, donor cells underwent apoptosis after implantation. Indeed, the TUNEL assay identified cells with fragmented DNA, indicative of apoptosis (Fig. 6A). Quantitation of TUNEL+ cells (green) revealed that the percentage of apoptotic cells at 1 wk was significantly higher in tissues containing donor SMCs (EC/SMC group: 33±2.7% vs. EC group: 5.23±5.76%, $p<0.01$, n=3) and were localized within the fibrin bands in between the SIS layers, where donor cells resided (Fig. 6B). The TUNEL+ cells decreased significantly at 1 mo (10.3±2.6%) and reached very low levels at 3 mo (4.8±1.3%). Finally, staining consecutive tissue sections of 1 mo EC/SMC grafts for TUNEL and for SRY/PCNA, respectively (Fig. 6C), showed that some SRY+ cells were proliferating (PCNA+) but others had fragmented DNA.

Evaluation of macrophage invasion into the implants

The presence of macrophages in the grafts was evaluated by immunostaining for AIF (red). Co-staining with calponin (CNN1, green) showed that CNN1+ cells were distinct from AIF + cells (Fig. 7A). Early infiltration of macrophages within the implanted grafts was observed within 1 wk, reaching maximum cell density at 1 mo (Fig. 7B, C). The number of incoming macrophages reduced at 3 mo as host cell density approached the density of native arteries. Macrophages were observed primarily close to the lumen (68.0±12.8%) and to a lesser extent also close to the transmural side (24.5±7.2%). Interestingly, the EC/SMC group exhibited higher macrophage densities at 1 wk and 1 mo compared to the EC group (Fig. 7C), which correlated with higher numbers of infiltrating cells at those times.

DISCUSSION

We report successful arterial implantation of tissue-engineered blood vessels manufactured using SIS-Fibrin hybrid biomaterial in an ovine carotid artery model up to 3 mo. In this pre-clinical assessment, our composite biomaterial exhibited time-dependent remodeling by host cells, leading to native artery-like architecture and function. Host cell infiltration was not restricted to the anastomotic sites but occurred through the luminal as well the extramural wall sides yielding uniform cell density throughout the graft by 1 mo post implantation. The presence of pre-seeded SMC in the vascular wall enhanced but was not necessary for host cell infiltration, remodeling and development of vascular function. The proliferation rate and the number of donor cells decreased over time *in-vivo*, suggesting that host cells dominated tissue remodeling, development of contractile function and integration of the grafts over time into the native tissue. This model adequately simulates human anatomy and pathologic processes and experimental success can be extrapolated to human physiology [21].

In a previous study from our laboratory, we demonstrated that an intact EC monolayer was necessary to prevent acute thrombosis of SIS-based vascular grafts using a short-term, arteriovenous shunt model [8]. Similar conclusions were reached by other studies using different biomaterials or animal models [22] [6, 23]. Therefore, EC were employed to cover the graft lumen and subjected to shear stress for several days to condition the cells to the hemodynamics of the arterial microenvironment. As a result, all grafts remained patent and each accommodated blood flow similar to that of the native carotid on the other side of the neck. In addition, SEM showed no platelet deposition and confirmed the presence of a completely homogeneous endothelial monolayer that was aligned in the direction of blood flow.

SIS is a porous collagen-based biodegradable material, which allows for maturation and growth and has been used as a tissue engineering scaffold [12–14]. In previous studies, SIS was used as a replacement for large diameter vena cava grafts in pigs [24] and as vascular patches supporting host cell infiltration [25, 26], but its performance as a small diameter arterial replacement graft has been inadequate [27], possibly due to lack of a functional endothelium. Our study showed that unlike vascular grafts based on decellularized arteries [7] or decellularized polymer based TEVs [5, 6], the endothelialized SIS-Fibrin scaffold yielded high patency rates (100%) and enabled significant repopulation by incoming host cells throughout the graft, even in the absence of donor SMCs. Indeed, at 3 mo post-implantation the vast majority of cells in the vascular wall came from the host, with donor cells accounting for only ~8% of total cells and 3% of all proliferating cells. This result shows that our TEVs enabled very high rates of cell infiltration throughout the length of the graft and not just at the anastomotic sites. It is unlikely that cells migrated from the anastomotic sites all the way to the middle of the graft, in such a short time. Indeed, measurements of cell density in the luminal (zone 1), intermediate (zone 2) and transmural (zone 3) areas of the middle section of grafts at 1 week post implantation suggested that cells may be coming from the luminal as well as the extramural wall sides. Cells infiltrating from the luminal side might have originated from circulating bone marrow progenitors as suggested by previous studies [28, 29], while cells coming from the extramural side might have been myofibroblasts.

TEVs were prepared with male cells and were implanted into female recipients thereby enabling monitoring of donor cell fate after implantation. Host cells infiltrated so fast, that by 1 mo post implantation, the donor (SRY+) cells constituted only ~17% of total cells in the vascular wall. The percentage of donor cells decreased further to ~8% by 3 mo post-implantation. At 1 mo the percentage of proliferating (PCNA+) cells within the SRY+ population was about 36%, which was comparable to that of the total cell population within the graft (~40% PCNA+ cells). At 3 mo post implantation, the percentage of PCNA+ cells in the total cell population decreased moderately to about 30% but the percentage of PCNA+ cells within the SRY+ population decreased more abruptly to ~13%. The decreased proliferation might be the result of graft maturation or perhaps the outcome of negative interactions between the host and donor cells. Indeed, the TUNEL assay showed that a significant percentage of donor cells underwent apoptosis, especially at 1 wk post implantation (~33% TUNEL+ cells). The reason for apoptosis of donor cells is unclear but the possibility that it might be due to immune attack by T cells can be excluded, as immunostaining for CD3 or CD20, showed no T or B cells in the graft (data not shown), as expected since the animals were immunosuppressed. Taken together, these results indicate that initially a significant fraction of donor cells experienced apoptosis while others continued to proliferate. Over time, proliferation of donor cells decreased and donor cells were outnumbered by the more proliferative incoming host cells, which became the dominant cell population and therefore, might be responsible for long-term remodeling and function of the vascular wall. In agreement with previous studies [30, 31], we found that SIS was remodeled successfully after implantation. At 1 wk, the mechanical properties (Young's modulus and UTS) of explanted grafts were lower than those of the pre-implanted TEVs. However, by 1 mo both YM and UTS increased significantly and by 3 mo they were similar to the levels of native arteries, even for TEVs that were initially devoid of cells in the medial wall. These results indicate that the SIS-Fibrin scaffold was remodeled rapidly by the infiltrating host cells and was replaced by new extracellular matrix e.g. collagen, ultimately enhancing the strength of the grafts to the level of native carotid arteries within a few weeks post implantation.

A particularly encouraging and unique outcome of our model is the uniformity of cell infiltration that was achieved after only 1 mo *in-vivo*. A circumferentially aligned muscle layer that was very similar in thickness and density to native tissue was established within the host regardless of the initial presence of SMC in the vascular wall. In contrast, when decellularized polymer based TEVs were implanted successfully in baboon, canine and porcine models, cell infiltration was limited to the anastomotic sites [5, 6]. On the other hand, when decellularized arteries were employed as TEV scaffolds, host cells were observed on the extramural wall side but infiltration into the grafts was also limited, especially in the absence of donor SMCs in the vascular wall [7]. Although the reasons for these differences are not clear, differences in material properties e.g. porosity and pore structure might have played a role. In addition, the presence of fibrin between the SIS layers might have promoted cell migration from the surrounding tissues, leading to uniform cell distribution. If this hypothesis is true, then incorporation of migration or differentiation promoting biological cues e.g. TGF-β1 [32] into the fibrin matrix, might further promote not only host cell infiltration but also faster maturation of the incoming cells. This would be

especially important for grafts lacking donor cells. Differences due to the animal species are less likely to account for the increased uniformity of cell infiltration, as sheep are similar to humans, dogs and baboons, exhibiting relatively high occlusion rates and low levels of endothelialization, which is restricted to the perianastomotic regions. Therefore, there is no reason to believe that cellular infiltration into the medial wall would be enhanced as compared to these other species. Indeed, one of the studies using decellularized arteries employed sheep but observed limited cell infiltration into the grafts [7].

Interestingly, by 1 mo post-implantation, all incoming cells expressed CNN1 indicating development of SMC phenotype. Notably, expression of SMC proteins αSMA, CNN1 and MYH11 was accompanied by development of vascular reactivity, which for some agonists, e.g. the thromboxane mimetic, U46619, was similar to that of native arteries. On the other hand, the response to KCl or ET-1 was significantly lower than that of native carotids, suggesting that the graft remodeling might still be incomplete. Nevertheless, maturation of incoming host cells into contractile SMCs, suggests that donor medial cells may not be necessary for generation of functional SIS-Fibrin grafts. This is important as isolation and expansion of SMCs to the numbers required for engineering arteries of clinically relevant length is time consuming and cell quality declines significantly with donor age and culture senescence [33–36]. Since the majority of patients in need of vascular grafts are elderly, bypassing the requirement for donor SMCs in the vascular wall may decrease the time and cost of TEV fabrication, thereby increasing their potential for clinical use.

Our study also shows that the course of remodeling follows the normal wound healing response, with infiltration of monocytes from the blood stream and resident macrophages from surrounding tissue within the first few days post-implantation. Recent studies demonstrated the importance of the inflammatory process and the transition of macrophages into M2 vs. M1 phenotype in transforming vascular grafts into functional neovessels [10, 37]. We observed macrophages infiltrating into the grafts from the lumen as well as the extramural wall. The number of AIF+ cells increased from 1 wk to 1 mo post-implantation but decreased thereafter, suggesting that the grafts might be approaching homeostasis. Co-staining with AIF and CNN1 showed that the two proteins were not co-localized in the same cells, suggesting that the two cell populations were independent. Interestingly, the number of macrophages was slightly higher in the EC/SMC grafts, possibly due to the presence of SMCs, which secrete potent monocytes/macrophages chemo-attractants, such as Monocyte Chemotactic Protein-1 (MCP-1). Interestingly, EC/SMC grafts also showed higher number of incoming cells than EC grafts at 1 mo post implantation. Collectively, these results suggest that macrophages may be critical for graft cellularization and remodeling, presumably by attracting host cells from the blood, the anastomotic sites, or the extramural wall to infiltrate the grafts. It will be interesting to deplete macrophages in our ovine animal model in order to test whether macrophage infiltration is necessary for successful remodeling of SIS-Fibrin grafts.

In summary, we report arterial implantation of SIS-Fibrin based grafts in a pre-clinical ovine animal model with 100% success rate. The SIS-Fibrin tissues provided microstructure that was amenable to infiltration by appropriate inflammatory and other host cells, leading to *in-vivo* maturation and development of vascular function. We also provided insight into the

role of pre-seeding donor medial cells into the TEVs and found that while medial cells increased the rate of host cell infiltration and graft remodeling, they were not necessary for graft remodeling or development of vascular contractile function. At 3 mo, the cell density in the vascular wall reached homeostatic levels but the ECM content and fibrous organization had not yet reached the native arterial level. Additional studies with longer times of implantation may show further improvement of graft function and provide additional insight into the long-term fate of donor cells. Finally, it will be interesting to follow the fate of donor ECs to elucidate whether these cells remain in the lumen or are replaced by host ECs - just like donor SMCs - thereby eliminating the need for long-term immune-suppression and possibly yielding higher long-term success rates of tissue engineered vascular grafts.

CONCLUSIONS

SIS-Fibrin biomaterial composite grafts have been successfully employed here as arterial replacement grafts in the carotid artery of a clinically relevant large animal model and evaluated for patency function and remodeling. Taken together, we report arterial implantation of bioengineered vascular grafts in a pre-clinical ovine animal model with 100% success rate. The SIS-Fibrin biomaterial provided microstructure that was amenable to infiltration by appropriate inflammatory and other host cells, leading to in-vivo maturation and development of vascular function. The encouraging results obtained from this ovine carotid model can be extrapolated to human physiology, addressing the need for arterial replacement grafts. This study demonstrates that SIS-Fibrin grafts without donor cells in the medial layer can function in-vivo raising the possibility for off-the-shelf design.

Supplementary Material

Refer to Web version on PubMed Central for supplementary material.

Acknowledgments

No persons are acknowledged in this work apart from the contributing authors.

This work was supported by grants from the National Heart and Lung Institute (R01 HL086582) and the New York Stem Cell Science Fund (NYSTEM, Contract# C024316) to S.T.A. and D.D.S.

References

1. Lundberg MS. Cardiovascular tissue engineering research support at the National Heart, Lung, and Blood Institute. Circ Res. 2013; 112(8):1097–103. [PubMed: 23580772]
2. Ravi S, Chaikof EL. Biomaterials for vascular tissue engineering. Regen Med. 2010; 5(1):107–20. [PubMed: 20017698]
3. Koch S, et al. Fibrin-polylactide-based tissue-engineered vascular graft in the arterial circulation. Biomaterials. 2010; 31(17):4731–9. [PubMed: 20304484]
4. Swartz DD, Russell JA, Andreadis ST. Engineering of fibrin-based functional and implantable small-diameter blood vessels. Am J Physiol Heart Circ Physiol. 2005; 288(3):H1451–60. [PubMed: 15486037]
5. Dahl SL, et al. Readily available tissue-engineered vascular grafts. Sci Transl Med. 2011; 3(68): 68ra9.

6. Quint C, et al. Decellularized tissue-engineered blood vessel as an arterial conduit. Proc Natl Acad Sci U S A. 2011; 108(22):9214–9. [PubMed: 21571635]
7. Neff LP, et al. Vascular smooth muscle enhances functionality of tissue-engineered blood vessels in vivo. J Vasc Surg. 2011; 53(2):426–34. [PubMed: 20934837]
8. Peng H, et al. A novel ovine ex vivo arteriovenous shunt model to test vascular implantability. Cells Tissues Organs. 2012; 195(1–2):108–21. [PubMed: 22005667]
9. Kapadia MR, et al. A reproducible porcine ePTFE arterial bypass model for neointimal hyperplasia. J Surg Res. 2008; 148(2):230–7. [PubMed: 18028957]
10. Roh JD, et al. Tissue-engineered vascular grafts transform into mature blood vessels via an inflammation-mediated process of vascular remodeling. Proc Natl Acad Sci U S A. 2010; 107(10): 4669–74. [PubMed: 20207947]
11. Wu W, Allen RA, Wang Y. Fast-degrading elastomer enables rapid remodeling of a cell-free synthetic graft into a neoartery. Nat Med. 2012; 18(7):1148–53. [PubMed: 22729285]
12. Lantz GC, et al. Small intestinal submucosa as a vascular graft: a review. J Invest Surg. 1993; 6(3): 297–310. [PubMed: 8399001]
13. Ferrand BK, et al. Directional porosity of porcine small-intestinal submucosa. J Biomed Mater Res. 1993; 27(10):1235–41. [PubMed: 8245038]
14. Hiles MC, et al. Porosity of porcine small-intestinal submucosa for use as a vascular graft. J Biomed Mater Res. 1993; 27(2):139–44. [PubMed: 8436570]
15. Wang ZQ, Watanabe Y, Toki A. Experimental assessment of small intestinal submucosa as a small bowel graft in a rat model. J Pediatr Surg. 2003; 38(11):1596–601. [PubMed: 14614707]
16. Gonzalez R, et al. Absorbable versus nonabsorbable mesh repair of congenital diaphragmatic hernias in a growing animal model. J Laparoendosc Adv Surg Tech A. 2011; 21(5):449–54. [PubMed: 21542768]
17. Phipatanakul WP, Petersen SA. Porcine small intestine submucosa xenograft augmentation in repair of massive rotator cuff tears. Am J Orthop (Belle Mead NJ). 2009; 38(11):572–5. [PubMed: 20049352]
18. Peng HF, et al. Hair follicle-derived smooth muscle cells and small intestinal submucosa for engineering mechanically robust and vasoreactive vascular media. Tissue Eng Part A. 2011; 17(7–8):981–90. [PubMed: 21083418]
19. Geer DJ, Swartz DD, Andreadis ST. Fibrin promotes migration in a three-dimensional in vitro model of wound regeneration. Tissue Eng. 2002; 8(5):787–98. [PubMed: 12459057]
20. Thomas SR, Chen K, Keaney JF Jr. Hydrogen peroxide activates endothelial nitric-oxide synthase through coordinated phosphorylation and dephosphorylation via a phosphoinositide 3-kinase-dependent signaling pathway. J Biol Chem. 2002; 277(8):6017–24. [PubMed: 11744698]
21. Byrom MJ, et al. Animal models for the assessment of novel vascular conduits. J Vasc Surg. 2010; 52(1):176–95. [PubMed: 20299181]
22. Schneider PA, et al. Preformed confluent endothelial cell monolayers prevent early platelet deposition on vascular prostheses in baboons. J Vasc Surg. 1988; 8(3):229–35. [PubMed: 3138436]
23. L'Heureux N, et al. A completely biological tissue-engineered human blood vessel. FASEB J. 1998; 12(1):47–56. [PubMed: 9438410]
24. Robotin-Johnson MC, et al. An experimental model of small intestinal submucosa as a growing vascular graft. J Thorac Cardiovasc Surg. 1998; 116(5):805–11. [PubMed: 9806387]
25. Boni L, et al. Reconstruction of pulmonary artery with porcine small intestinal submucosa in a lamb surgical model: Viability and growth potential. J Thorac Cardiovasc Surg. 2012; 144(4):963–969 e1. discussion 969. [PubMed: 22917684]
26. Padalino MA, et al. Extracellular matrix graft for vascular reconstructive surgery: evidence of autologous regeneration of the neoaorta in a murine model. Eur J Cardiothorac Surg. 2012; 42(5):e128–35. [PubMed: 22912435]
27. Pavcnik D, et al. Angiographic evaluation of carotid artery grafting with prefabricated small-diameter, small-intestinal submucosa grafts in sheep. Cardiovasc Intervent Radiol. 2009; 32(1): 106–13. [PubMed: 18931872]

28. Shimizu K, et al. Host bone-marrow cells are a source of donor intimal smooth- muscle-like cells in murine aortic transplant arteriopathy. Nat Med. 2001; 7(6):738–41. [PubMed: 11385513]
29. Diao Y, et al. Long-term engraftment of bone marrow-derived cells in the intimal hyperplasia lesion of autologous vein grafts. Am J Pathol. 2008; 172(3):839–48. [PubMed: 18276778]
30. Helton WS, et al. Short-term outcomes with small intestinal submucosa for ventral abdominal hernia. Arch Surg. 2005; 140(6):549–60. discussion 560–2. [PubMed: 15967902]
31. Sclamberg SG, et al. Six-month magnetic resonance imaging follow-up of large and massive rotator cuff repairs reinforced with porcine small intestinal submucosa. J Shoulder Elbow Surg. 2004; 13(5):538–41. [PubMed: 15383811]
32. Liang MS, Andreadis ST. Engineering fibrin-binding TGF-beta1 for sustained signaling and contractile function of MSC based vascular constructs. Biomaterials. 2011; 32(33):8684–93. [PubMed: 21864893]
33. Koobatian MT, et al. Differential effects of culture senescence and mechanical stimulation on the proliferation and leiomyogenic differentiation of MSC from different sources: implications for engineering vascular grafts. Tissue Eng Part A. 2014
34. Han J, et al. Nanog reverses the effects of organismal aging on mesenchymal stem cell proliferation and myogenic differentiation potential. Stem Cells. 2012; 30(12):2746–59. [PubMed: 22949105]
35. Bajpai VK, Mistriotis P, Andreadis ST. Clonal multipotency and effect of long-term in vitro expansion on differentiation potential of human hair follicle derived mesenchymal stem cells. Stem Cell Res. 2012; 8(1):74–84. [PubMed: 22099022]
36. Han J, et al. Molecular and functional effects of organismal ageing on smooth muscle cells derived from bone marrow mesenchymal stem cells. Cardiovasc Res. 2010; 87(1):147–55. [PubMed: 20097675]
37. Hibino N, et al. A critical role for macrophages in neovessel formation and the development of stenosis in tissue-engineered vascular grafts. FASEB J. 2011; 25(12):4253–63. [PubMed: 21865316]

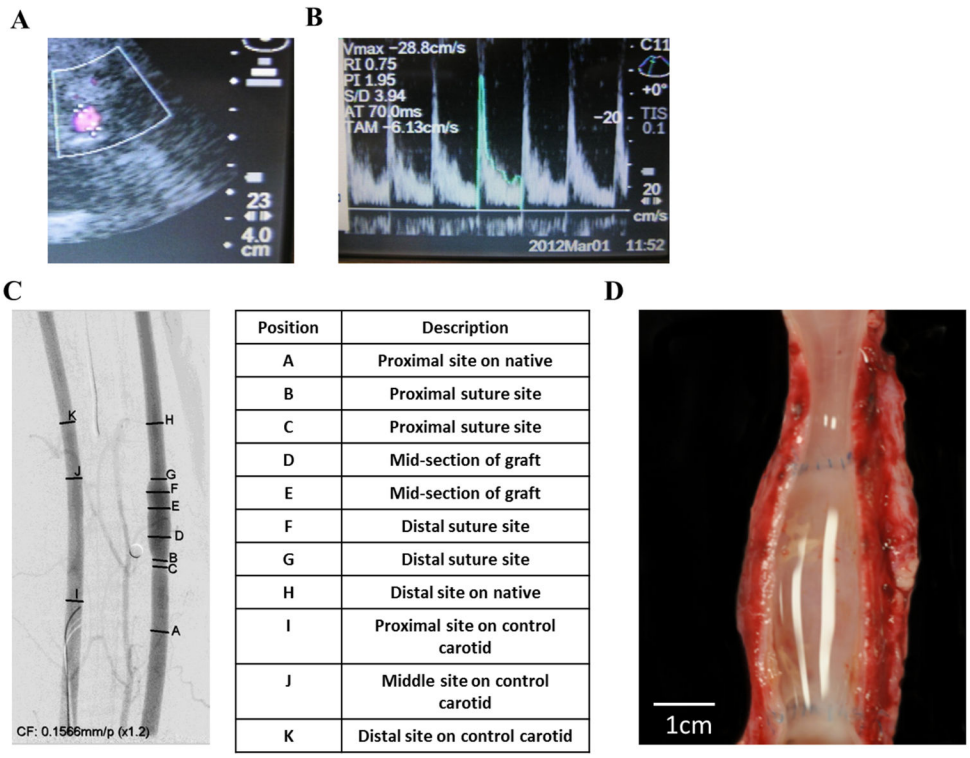

Position	Description
A	Proximal site on native
B	Proximal suture site
C	Proximal suture site
D	Mid-section of graft
E	Mid-section of graft
F	Distal suture site
G	Distal suture site
H	Distal site on native
I	Proximal site on control carotid
J	Middle site on control carotid
K	Distal site on control carotid

Figure 1. Monitoring patency of implanted TEV

(A) Ultrasonography of TEV. (B) Flow profile through the implanted TEV. (C) Angiography at 3 mo post-implantation. The table shows proximal, distal and anastomosis sites of implanted TEVs from the corresponding angiographic image. (D) Gross images of explanted TEV at 3 mo exhibiting a clean, patent lumen.

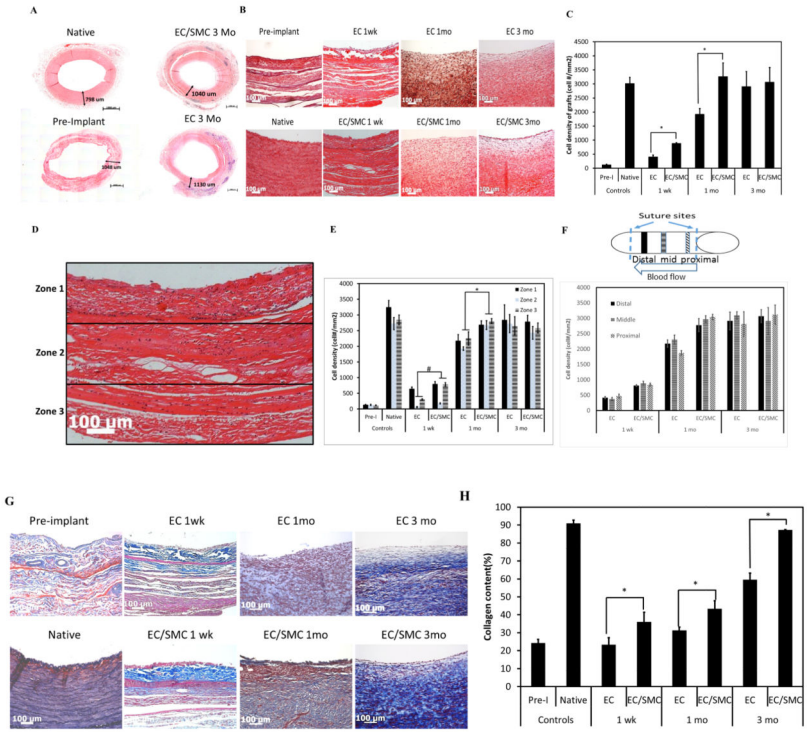

Figure 2. Histological examination of explanted TEVs

(A) H&E images of TEV ring sections. Each number represents wall thickness. Bar: 1000 µm. (B) H&E staining of cross-sections of explanted TEVs at the indicated times. Bar: 100 µm. (C) Quantification of cell density using Image J (*: $p<0.05$, n=3; 5 tissue sections per graft for 3 grafts). (D) Each H&E image was divided into three zones indicating the luminal, extramural and intermediate section of each graft. Bar: 100 µm. (E) Cell density in each zone at the indicated times (#: $p<0.03$; *: $p<0.05$). (F) Cell density in the distal end, mid-section and proximal end of each graft at the indicated times. The schematic shows the proximal, middle and distal sections of the graft. (G) Masson's Trichrome staining of explanted grafts at the same time points. Bar: 100 µm. (H) Quantification of collagen staining intensity (blue) using Image J (*: $p<0.05$, n=3).

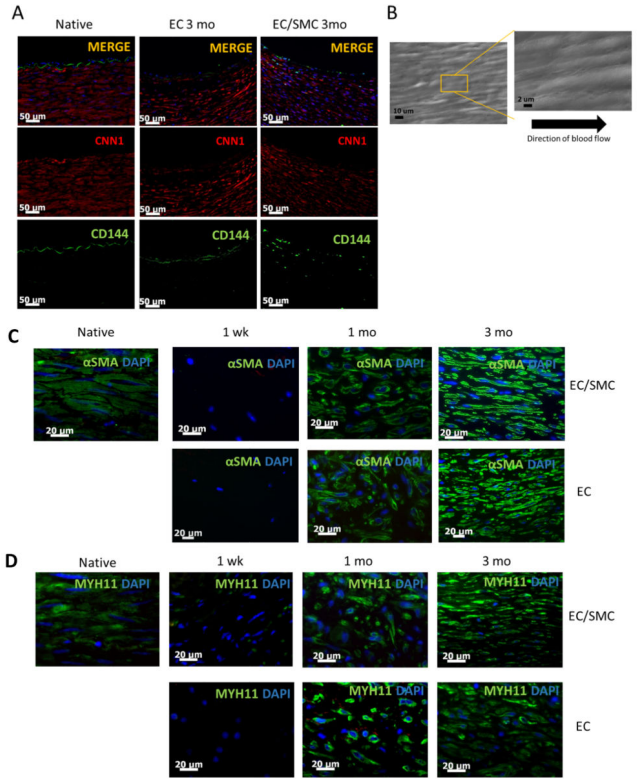

Figure 3. Immunohistochemistry and SEM

(A) Immunostaining of tissue sections of explanted grafts (3 mo) or native arteries for CD144 (green) or CNN1 (green). Nuclei were counterstained with DAPI (blue). Bar= 50 μm. (B) SEM en-face of explanted tissue showing confluent endothelial monolayer aligned in the direction of blood flow. (C) Immuno-staining for αSMA (green) or (D) MYH11 (green) of graft sections at the indicated times. Native artery served as control. Nuclei were counterstained for DAPI (blue). Bar= 20 μm.

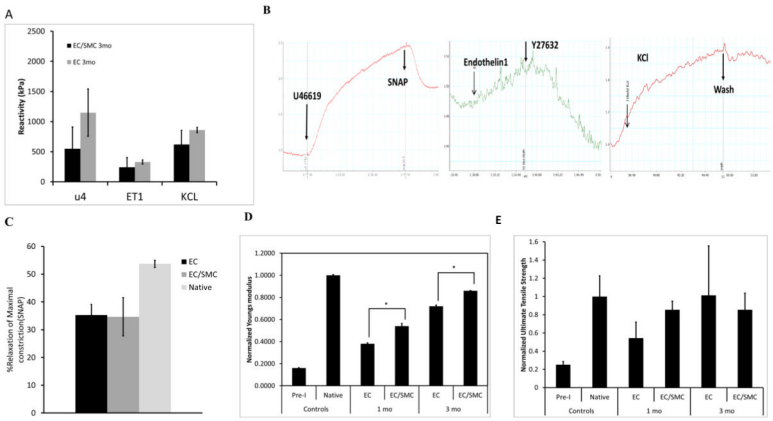

Figure 4. Contractility and mechanical properties of explanted TEVs

(A) Vascular reactivity of explanted TEVs from EC/SMC or EC TEVs at 3 mo in response to the indicated agonists. (B) Signature force-time curves upon addition of vaso-constrictors (U46619, ET-1 and KCL) or vasodilators (SNAP, Y27632). (C) Young's modulus of explanted TEVs normalized to the corresponding values of native carotids (*: $p<0.05$, n=3). (D) Ultimate Tensile Strength of explanted TEVs normalized to the corresponding values of native carotids.

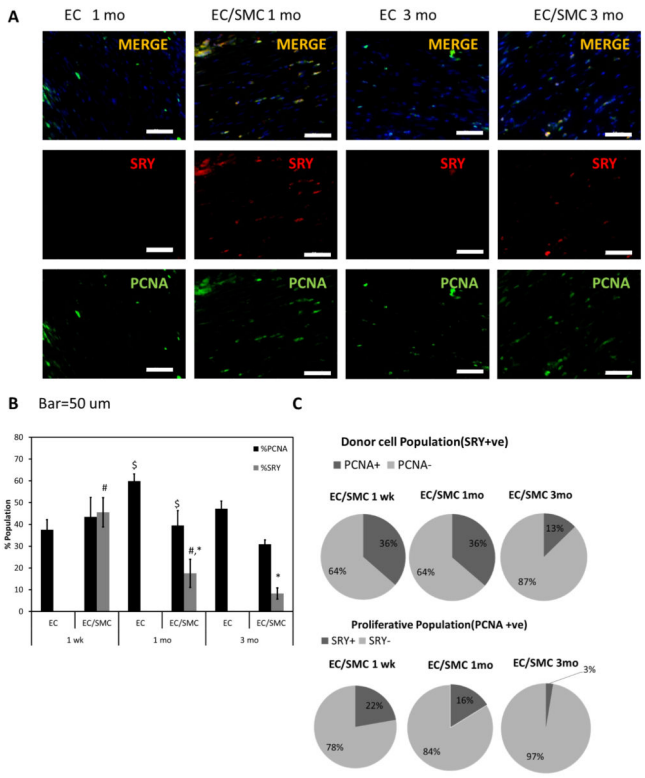

Figure 5. Evaluation of donor cell retention

(A) Immunostaining for SRY (red) and PCNA (green). Bar: 50 μm. (B) Percentage of SRY+ (donor) and PCNA+ (proliferating) cells in EC or EC/SMC TEVs at 1 mo and 3 mo (#, *, $: $p<0.05$, n=3). (C) Pie charts show %SRY+ cells within the proliferative population of PCNA+ cells and PCNA+ cells within the SRY+ (donor) cell population.

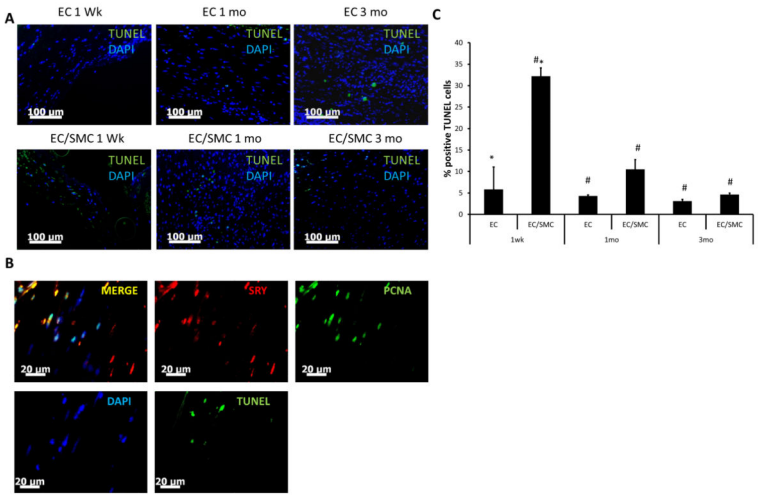

Figure 6. Evaluation of apoptotic cells within the vascular grafts

(A) TUNEL assay was performed on paraffin sections of explanted TEVs. TUNEL positive nuclei appear green; nuclei were counterstained with DAPI (blue). Bar=100 μm. (B) Top panel: immunostaining of 1 wk explanted TEVs for SRY (red) and PCNA (green) (TOP panels). Bottom panel: TUNEL+ nuclei (green) in a consecutive tissue section; nuclei were counterstained with DAPI (blue). Bar= 20 μm. (C) Quantification of TUNEL+ nuclei as percentage of total (DAPI+) nuclei (#: $p<0.02$, *: $p<0.05$, n=3).

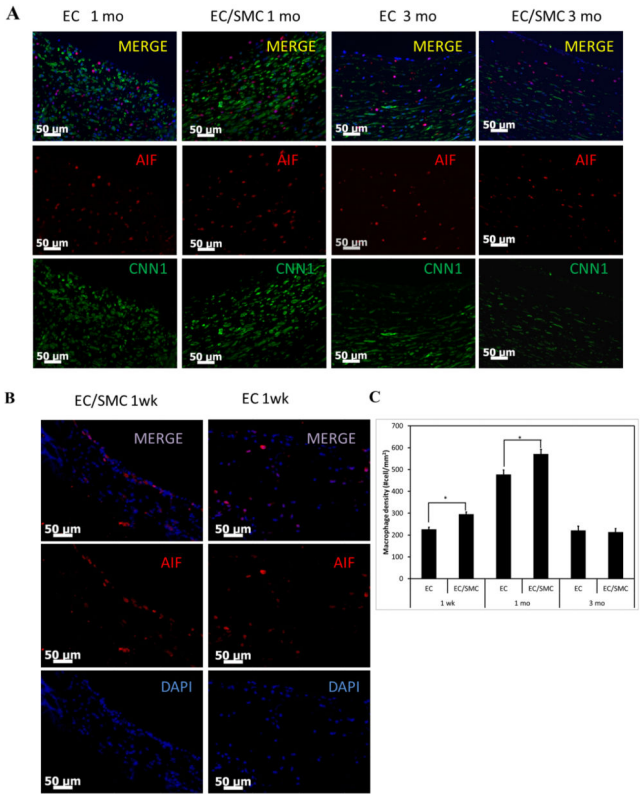

Figure 7. Macrophage invasion into implanted TEVs

(A) Immuno-staining of explanted tissue cross-sections at 1 mo and 3 mo EC and EC/SMC TEVs for AIF (red) and CNN1 (green). Nuclei were counterstained with DAPI (blue). Bar: 50 μm. (B) Early macrophage infiltration is shown in 1 wk explanted EC and EC/SMC TEVs. (C) Quantification of macrophage invasion reported as cell density/mm^2 of cross-sectional area (*=$p<0.05$, n=3).